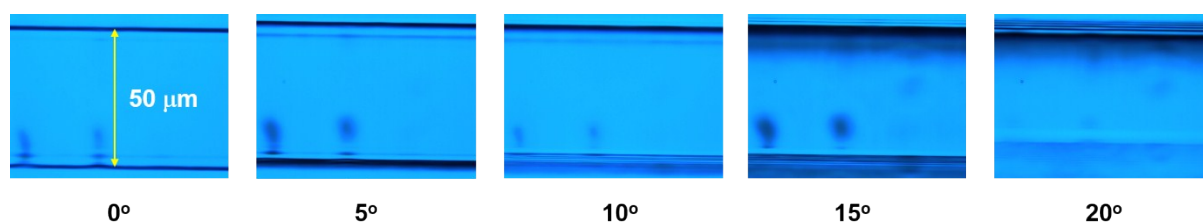


## Supplementary Information

### Alignment of the High-pressure Silica Capillary in the Focal Volume of the Fluorescence Microscope

The coupling unit connecting capillary and pressure plug to the high pressure tubing is kept in a translation table which has a horizontal, vertical and turning screw, allowing us to find the optimized focal position of the capillary (see Figure 1). The turning screw is very important as it allows free rotation of the capillary around its longitudinal axis, thus allowing perfect capillary alignment in the focal plane. In an inclined capillary, the refraction of light deforms the point spread function (PSF), and the focal spot is shifted to a different position compared to the planar geometry. Figure S1 shows contrast images of a perfectly planar and an inclined capillary. We used the molecular fluorescence brightness ( $\eta$ ) of the Atto 565 and Atto 647N dyes as a parameter to demonstrate the effect of inclination angle on the performance of our high-pressure setup.  $\eta$  has been calculated from the photon count rate histogram (PCH) and FCS curve. PCH provides the average counts ( $k$ ), and from the amplitude of the FCS curve at correlation time zero,  $G(0)$ , the number of molecules ( $N$ ) in the confocal volume is obtained ( $G(0) = 1/N$ ), to yield  $\eta = G(0) k$ , that is counts per molecule. Figure S2 depicts  $\eta$ -values of Atto 565 and Atto 647N as a function of inclination angle ( $\alpha$ ). Within  $\alpha = \pm 5^\circ$ ,  $\eta$  remains essentially constant, at larger angles,  $\eta$  decreases markedly with increasing  $\alpha$  due to the misalignment of the focal spot with respect to the pinhole. Moreover, the focal spot gets distorted due to refraction from side planes of the inclined capillary.



**Figure S1:** Phase contrast images of the inner surface of the capillary at different inclination angles ( $\phi$ ). The black solid lines observed for the truly parallel capillary ( $\phi = 0^\circ$ ) represent the top and bottom inner surface of the capillary. As  $\phi$  increases, the solid lines begin to fade and are not distinguishable anymore for a largely inclined capillary. The dimension of the inner bore of the capillary is 50  $\mu\text{m}$ .

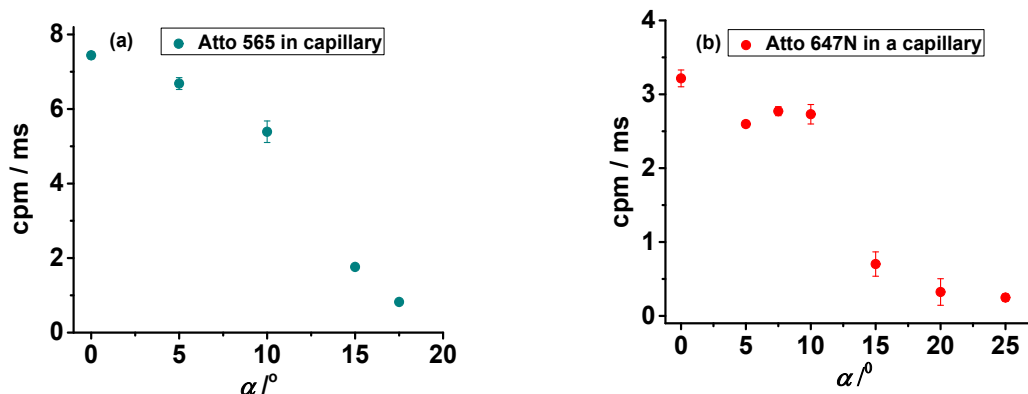


**Figure S2:** Plot of the brightness ( $\eta$ ), which is counts per molecule per ms (cpm/ms), as a function of inclination angle of the capillary for (a) Atto 565 and (b) Atto 647N. With increasing inclination angle, the molecular brightness decreases.

We also checked the effect of focal depth on the PSF by looking at the  $\eta$  value at different  $z$  positions in the inner bore of the capillary while the capillary is perfectly planar in the focal plane. The bottom inner surface of the capillary, which can be imaged from the back reflection light using a CCD camera, served as the origin of the  $z$  axis. We mapped almost the entire inner bore (50  $\mu\text{m}$ ) of the capillary using the focussing wheel of the microscope. Figure S3 shows the  $\eta$  values as a function of  $z$  from the inner surface of the capillary. The  $\eta$  value changes negligibly up to 30  $\mu\text{m}$  from the inner bottom surface of the capillary. Noticeable changes, though not drastic, are observed very close to the inner top surface of the capillary. These results indicate that refraction of the light due to different refractive indices between water and the fused silica surface of the capillary induce minimum optical aberration compared to that of a cylindrical shaped capillary along the optical axis inside the capillary.<sup>1</sup>

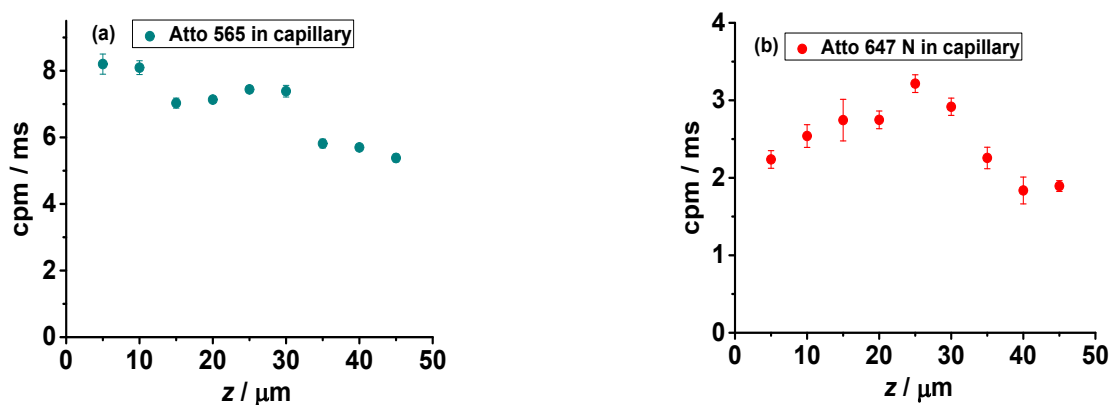


**Figure S3:** Molecular brightness ( $\eta$ ), in cpm/ms, of (a) Atto 565 and (b) Atto 647N at different  $z$  positions from the inner surface of the capillary. The bottom inner surface of the capillary serves as the origin of the  $z$  axis. We imaged the bottom inner surface of the capillary through the back reflection light using a CCD camera. The laser focus is moved along the optical axis using a focussing knob where 1 scale division is 1  $\mu\text{m}$ .

## Determination of the PSF in Capillary and Coverslip

The point spread function, PSF, represents the intensity distribution at the focal spot and therefore determines the shape and dimensions of the confocal volume. The confocal volume or PSF can be determined in two ways.<sup>2,3</sup> Either indirectly from the FCS measurement by monitoring the diffusion coefficient of a standard fluorophore in water, or directly using imaging of sub-resolution fluorescent beads (0.1  $\mu\text{m}$  in our case).<sup>2</sup> These sub- $\mu\text{m}$  fluorescent beads can be treated as a point source and can therefore be used to map the confocal volume. Since these microsphere beads are labelled with various fluorophores, they can be imaged at a broad variety of excitation wavelengths, allowing us to image the focal volume for both donor and acceptor excitation. We also imaged the PSF in both the donor and acceptor channel to determine the focal overlap in both the channel. The beads were immersed in a 40 wt% glycerol solution to minimize movement of the beads. Images are taken in the  $xy$  plane using a  $xy$  piezo scanner (P733.2CL, Physik Instruments) (Figure S4). The intensity distribution of these images in  $x$  and  $y$  direction are fitted into a single peak Gaussian distribution to determine the dimensions of the confocal volume in  $x$  and  $y$  direction (Figure S5). The dimensions of the confocal volume is defined as the radius where the maximum intensity at the centre decreases to its  $1/e^2$  value. The  $1/e^2$  radius in the  $x$ ,  $y$  and  $z$  direction is represented by  $\omega_x$ ,  $\omega_y$  and  $\omega_z$ , respectively. The integrated area of these  $xy$  images are taken at different  $z$  positions to determine the  $z$  profile of our confocal volume (Figs. S6 and S7). Table S1 shows the results and the comparison with corresponding coverslip data for both donor (560 nm) and acceptor (635 nm) excitation. From these data it is apparent that the PSF is more elongated in the  $z$  direction in case of the capillary compared to the coverslip. The confocal volume for coverslip and capillary is drawn in Figure S8 based on the values of  $1/e^2$  radii. Using the values of  $1/e^2$  radii, we determined the effective observation volume,  $V_{\text{eff}} = \pi^{3/2} \omega_x \omega_y \omega_z$ , and obtained  $V_{\text{eff}}$  values at 560 nm of  $1.6 \pm 0.4$  fL and  $0.8 \pm 0.2$  fL for capillary and coverslip, respectively (at 635 nm of  $1.9 \pm 0.4$  fL and  $0.9 \pm 0.3$  fL, respectively). We also examined the focal overlap between detector 1 (acceptor channel) and detector 2 (donor channel). Figure S9 shows the images of the beads in the capillary obtained from detector 1 and detector 2. The position of the beads in the image remains almost the same, indicating good overlap between detectors 1 and 2.

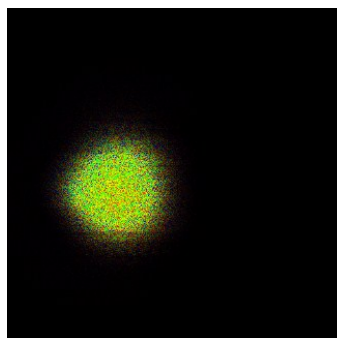
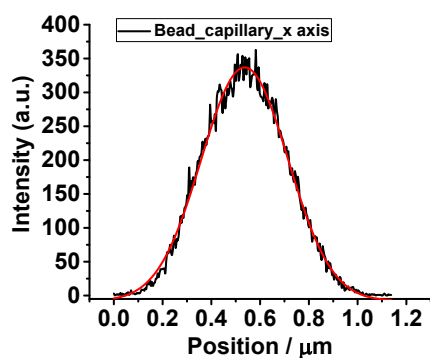


**Figure S4:** Images of the tetraspek beads in the  $xy$  focal plane inside the capillary. The intensity distribution along the  $x$  and  $y$  axis are used to determine the radius in  $x$  ( $\omega_x$ ) and  $y$  direction ( $\omega_y$ ), respectively. The frame size of the image is  $2 \mu\text{m} \times 2 \mu\text{m}$ . The excitation wavelength ( $\lambda_{\text{ex}}$ ) is 560 nm.

a)



b)

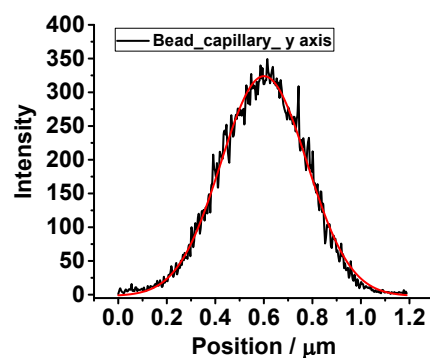


**Figure S5:** Intensity distribution along the (a)  $x$  and (b)  $y$  axis of the beads. The intensity distribution is fitted to a single peak Gaussian distribution to determine the  $1/e^2$  radius in  $x$  and  $y$  direction, respectively.

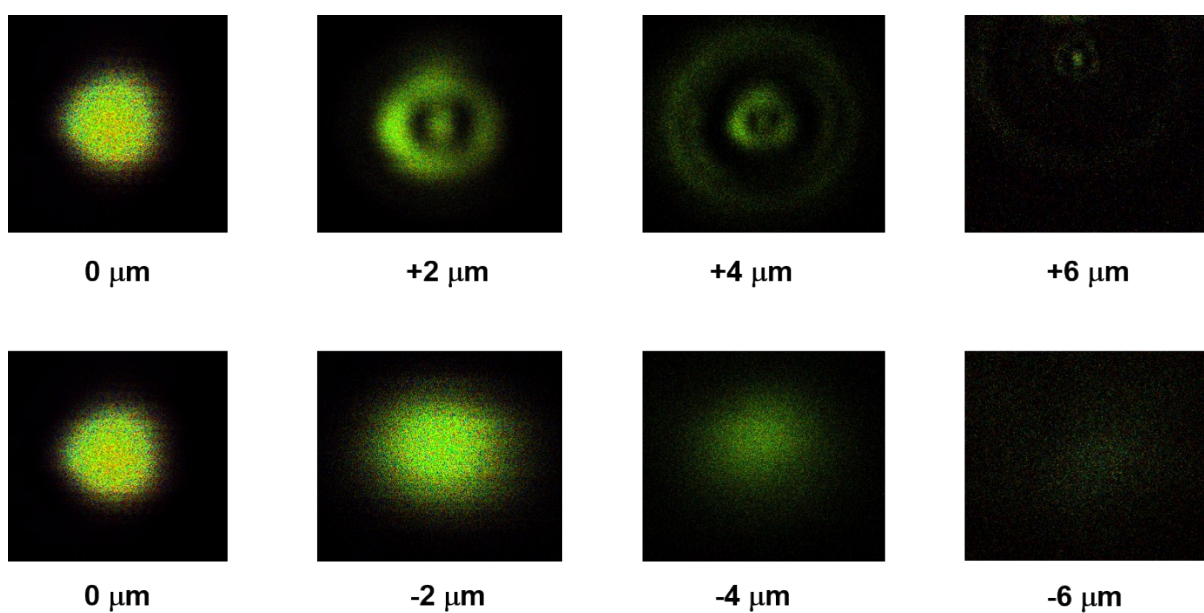


**Figure S6:** Images of the beads in the  $xy$  focal plane inside the capillary at different  $z$  positions. The top and bottom panels represent images obtained at different  $z$  positions above and below the focus, respectively. The integrated intensity of the images was used to obtain the  $z$  profile of the focal volume. The excitation wavelength ( $\lambda_{\text{ex}}$ ) is  $560 \text{ nm}$ .

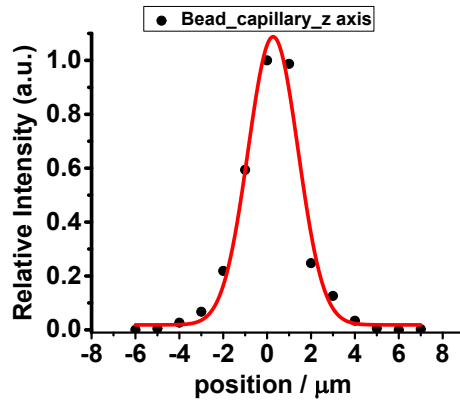


**Figure S7:** Intensity distribution along the  $z$  axis of the bead shown in Figures S4 and S6. The integrated intensities of the  $xy$  plane at different  $z$  position were used to obtain the intensity distribution along the  $z$  axis. The intensity is normalized to the data for  $z = 0$ . The intensity distribution is fitted to a single peak Gaussian distribution to obtain the axial radius ( $\omega_z$ ) of the focal volume. The excitation wavelength ( $\lambda_{\text{ex}}$ ) is 560 nm.

**Table S1:** Dimensions of the confocal volume on coverslip and in the capillary obtained from the tetraspeck bead measurement.  $\omega_x$ ,  $\omega_y$  and  $\omega_z$  represent the  $1/e^2$  radii in the  $x$ ,  $y$  and  $z$  direction of the focal volume.

Excitation wavelength	$1/e^2$ radii	Cover slip	Capillary
560 nm	$\omega_x$	$0.252 \pm 0.035 \mu\text{m}$	$0.365 \pm 0.040 \mu\text{m}$
	$\omega_y$	$0.501 \pm 0.055 \mu\text{m}$	$0.361 \pm 0.030 \mu\text{m}$
	$\omega_z$	$1.080 \pm 0.090 \mu\text{m}$	$2.170 \pm 0.170 \mu\text{m}$
635 nm	$\omega_x$	$0.255 \pm 0.035 \mu\text{m}$	$0.386 \pm 0.035 \mu\text{m}$
	$\omega_y$	$0.505 \pm 0.040 \mu\text{m}$	$0.382 \pm 0.025 \mu\text{m}$
	$\omega_z$	$1.200 \pm 0.100 \mu\text{m}$	$2.280 \pm 0.200 \mu\text{m}$

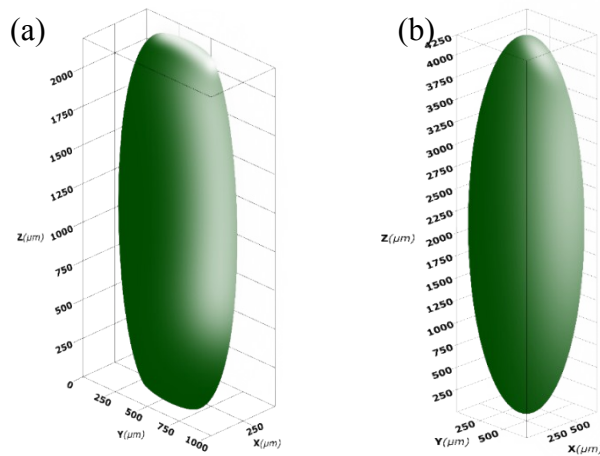


**Figure S8:** Picture of the focal volume on the coverslip (a) and in the capillary (b), according to the results of the microsphere measurement. On the coverslip, the  $xy$  plane was measured to be elliptical with a ratio  $\omega_x/\omega_y = 1/2$ .

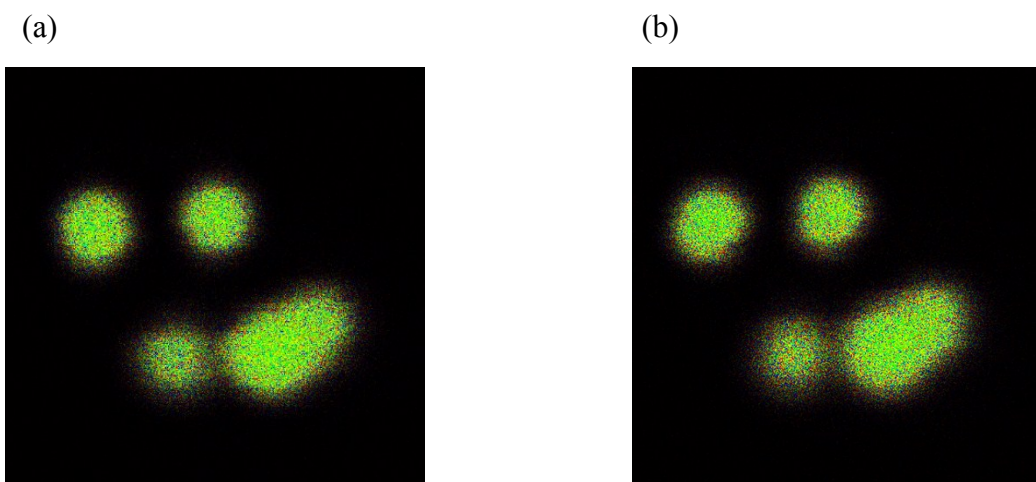


**Figure S9:** Fluorescence image of 0.1  $\mu\text{m}$  tetraspeck beads at 635 nm excitation inside the square-shaped capillary at (a) detector 1 (acceptor channel) and (b) detector 2 (donor channel). The frame size of the image is 3.8  $\mu\text{m}$  x 3.8  $\mu\text{m}$ . The positions of the beads in the images (a) and (b) are more or less the same, indicating good focal overlap in detector 1 and detector 2, which is crucial for a successful FRET measurement.

### FCS Measurements of Standard Fluorophores on the Coverslip and in the Capillary

We also conducted comparative FCS measurements on the Atto 565 and Atto 647N dye in a capillary and on coverslip at both donor (560 nm) and acceptor excitation (635 nm). The  $V_{\text{eff}}$  obtained from FCS measurements using the known diffusion coefficient ( $D$ ) of Atto 565 as 259  $\mu\text{m}^2 \text{s}^{-1}$ , is  $0.8 \pm 0.1$  fL and  $1.7 \pm 0.1$  fL for the cover slip and capillary, respectively, for 560 nm excitation.<sup>4</sup> The  $V_{\text{eff}}$  values are  $1.0 \pm 0.1$  fL and  $2.0 \pm 1.0$  fL for the coverslip and capillary, respectively, as determined from the  $D$ -value of Cy 5 ( $360 \mu\text{m}^2\text{s}^{-1}$ ) for 635 nm excitation.<sup>4</sup> The  $V_{\text{eff}}$  value obtained from the FCS measurement is in good agreement with the bead measurements. A larger  $\kappa$  value, defined as  $\kappa = \omega_z/\omega_{xy}$ , is also observed for the capillary ( $\kappa = 9$  for the capillary,  $\kappa = 9$  for the cover slip geometry). This is also consistent with the bead measurements where we found that in case of the capillary, the observation volume is elongated in the  $z$  direction. The results of the FCS measurements obtained for Atto 565 and Atto 647N in a capillary and on coverslip are displayed in Table S2. The molecular brightness ( $\eta$ ) value in case of the capillary is 4-5 times lower compared to that observed on cover slip. This could be due to a lower photon flux density as the observation volume gets bigger in the capillary. Another possible reason could be that some of the light is lost due to refraction from the side plane of the capillary.

**Table S2:** Fluorescence parameters of the fluorophore Atto 550 and Ato 647N as obtained from the FCS measurements on the coverslip and in the capillary.

Fluorophore	$\lambda_{\text{ex}} / \text{nm}$	Parameters	Cover slip	Capillary
Atto 550	560	$\langle C \rangle / \text{nM}$	$0.40 \pm 0.04$	$0.56 \pm 0.01$
		$\langle N \rangle$	$0.17 \pm 0.02$	$0.56 \pm 0.03$
		$\eta / (\text{cpm}/\text{ms})$	$29.4 \pm 0.6$	$7.44 \pm 0.09$
		$V_{\text{eff}} / \text{fL}$	$0.8 \pm 0.1$	$1.7 \pm 0.1$
		$\kappa$	$6.0 \pm 1.0$	$9.0 \pm 1.5$
Atto 647N	635	$\langle C \rangle / \text{nM}$	$4.7 \pm 0.3$	$4.2 \pm 0.2$
		$\langle N \rangle$	$2.76 \pm 0.40$	$4.95 \pm 0.21$
		$\eta / (\text{cpm}/\text{ms})$	$12.6 \pm 0.2$	$3.21 \pm 0.11$
		$V_{\text{eff}} / \text{fL}$	$1.0 \pm 0.1$	$2.0 \pm 0.1$
		$\kappa$	$6 \pm 1.5$	$9 \pm 2$

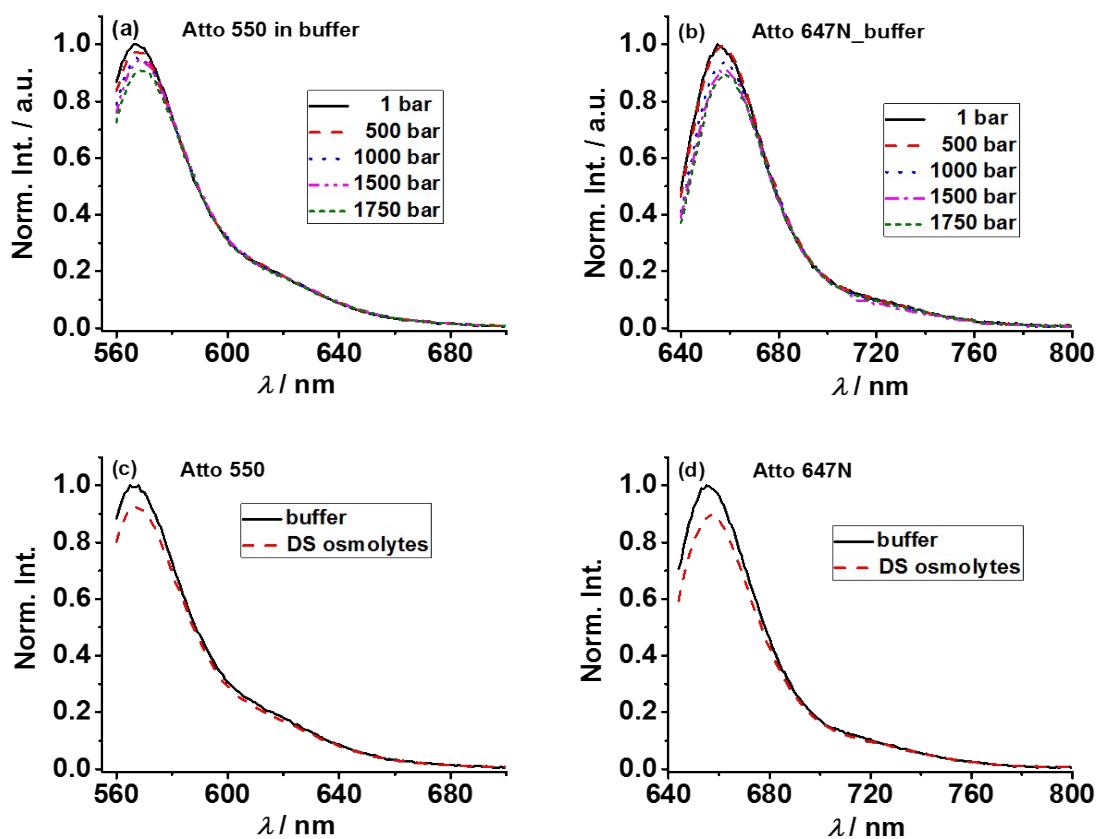


**Figure S10:** Emission spectra of (a) Atto 550 and (b) Atto 647N in buffer at different pressures. Effect of the deep sea (DS) osmolyte mixture on the emission spectrum of (c) Atto 550 and (d) Atto 647 N in comparison to neat buffer.

## References

1. J. D. Müller and E. Gratton, *Biophys. J.*, 2003, **85**, 2711–2719.
2. V. Buschmann, B. Krämer, F. Koberling, R. Macdonald and S. Rüttinger, *Application note*, 2009, PicoQuant GmbH,  
[https://www.picoquant.com/images/uploads/page/files/7351/appnote\\_quantfcs.pdf](https://www.picoquant.com/images/uploads/page/files/7351/appnote_quantfcs.pdf);
3. S. Rüttinger, *Confocal Microscopy and Quantitative Single Molecule Techniques for Metrology in Molecular Medicine*, Technical University Berlin, 2007, Dissertation, available at: [https://depositonce.tu-berlin.de/bitstream/11303/1796/1/Dokument\\_6.pdf](https://depositonce.tu-berlin.de/bitstream/11303/1796/1/Dokument_6.pdf);
4. P. Kapusta, *Application note*, 2010, PicoQuant GmbH,  
[https://www.picoquant.com/images/uploads/page/files/7353/appnote\\_diffusioncoefficient\\_s.pdf](https://www.picoquant.com/images/uploads/page/files/7353/appnote_diffusioncoefficient_s.pdf)